Vinh-Quan Nguyen, Quang-Tho Tran*

J. Electrical Systems 19-1 (2023): 111-134

Regular paper

Phase modulation of carriers for cascaded multilevel three-phase inverters

Cascaded multilevel three-phase inverters are commonly used in industrial applications and the quality of these inverters is highly dependent on the modulation techniques. The common mode voltage is one of the factors affecting the quality of the three-phase inverter output voltage. This paper proposes a carrier phase modulation method for cascade multilevel inverters to reduce the magnitude of common-mode voltage magnitude and harmonics. In the proposed method, the carrier phase modulator is considered as an adaptive controller and the phase of carrier is completely controlled by the magnitude of control signal. The phase modulation has a high immunity to the noises compared with the modulations of frequency and amplitude because it is difficult for noises to intrude into the phase of carrier. In addition, the algorithm of carrier phase modulation is simple and requires little memory. Moreover, the number of switching commutations of the proposed method also reduces significantly. Simulation and experiment results based on a cascaded five-level three-phase inverter system have confirmed the effectiveness of the proposed method compared with that of the popular methods using unmodulated carriers such as phase disposition (PD) and phase opposite disposition (POD).

Keywords: Carrier modulation; cascaded multilevel inverter; common-mode voltage; total harmonic distortion; phase disposition.

1. Introduction

Cascaded multilevel three-phase inverters (CMIs) have been widely used in industrial fields [1]–[6] due to their ability to withstand high voltage and large capacity applications [7], [8]. Particularly, in the grid-connected converters and active power filters, the multilevel inverters are capable of withstanding voltage shock when disconnected or connected to the grid. In addition, they are capable of offering a sinusoidal output voltage and lower transistor voltage shock which makes devices more durable [9]–[11]. However, the higher the number of levels, the more power devices must be used. Then, the higher the probability of error is. Moreover, the power quality of the inverter output voltage is highly dependent on the modulation technique. There are many groups of modulation commonly used. These are the space vector modulation techniques [12] and the level comparison techniques of sinusoidal pulse width modulation (SPWM) using the carriers. In the space vector modulation techniques, the number of states increases significantly according to the level of inverters [12]. Thus, this requires the powerful and expensive hardware. In the existing SPWM methods, the control signal is compared directly with the carriers [13]–[16] by using the comparison of levels. Therefore, these methods are simple and do not need the powerful hardware. However, the independence between the control signal and the carriers makes the carriers uncontrollable by any quantity. Furthermore, the common modulation techniques such as: phase disposition (PD) and phase opposite disposition (POD) are commonly used in the CMIs and use the constant carriers [17]. These carriers do not contain any information of the control signal. Therefore, it is very difficult for the modulator to reproduce the inverter output voltage as expected. This is

* Corresponding author: Quang-Tho Tran, Faculty of Electrical and Electronics Engineering, Ho Chi Minh city University of Technology and Education, Ho Chi Minh city, Vietnam, Email: thotq@hcmute.edu.vn

even more evident for the high-power inverters that often use the low-frequency carriers to reduce switching losses. Moreover, the existence of common mode voltage (CMV) in the CMIs is unavoidable. However, the high magnitude of the CMV is the factor adversely affecting the long life of the electric motors connected to the inverters. The CMV also causes high frequency noise and motor leakage current to affect the electrical equipment working near the motor [18], [19]. For grid-connected transformer-less inverter systems using renewable energies [20], the CMV generates the leakage currents and injects the harmonic currents into the power grid.

There are many proposed solutions to improve the quality of inverter output voltage using the strategies to reduce CMV [21]–[25]. However, the increase of the carrier frequency causes the memory size and switching loss to increase. The CMV suppression methods in [26], [27] are used for neutral point clamp inverters and space vector modulation. They have not been used for the CMIs. Similarly, the techniques in [28]–[30] using the control signals and the carrier frequency modulation have also not been applied for the CMIs. In addition, these techniques require a powerful and expensive hardware. This also causes difficulty to implement in reality due to the limits of common power devices. The method in [31] using the control signal modulation has not considered the effects of the CMV.

The technique of carrier phase modulation has been widely used in communications [32]–[38]. In this technique, the phase of carrier is modulated according to the control signal magnitude. Then, these carriers are called the phase modulated carriers. The advantage of this technique is that it is efficient in reconstructing the information of the control signal. However, this technique has not been used in the modulation for the CMIs. The adaptive transformation of the carrier phase according to the amplitude of the control signal makes switches easily reproduce the control signal at the output of the inverters. This can also help the low-frequency carriers improve the power quality of the inverter output voltage.

In most CMIs, the PD and POD techniques [17], [39], [40] use the constant carriers in the modulation. This paper proposes a carrier phase modulation (PM) method to reduce the CMV magnitude of the CMIs. In the proposed method, the phase of the carrier is modulated according to the control voltage amplitude for each phase. The lower CMV magnitude of the PM method helps reduce the total harmonic distortion (THD) of the inverter output voltage. The simulation and experimental results are performed based on a cascaded five-level three-phase inverter system. To evaluate the effectiveness of the proposed PM method, the quantities of this method such as the CMV and THD are also considered when compared with the those of the PD and POD methods. Furthermore, the general control formulas are also presented for the n-level inverters.

A model of the cascaded five-level H-bridge three-phase inverter is described in Section 2. The unmodulated carrier approach is also presented in Section 3. The carrier phase modulation method is presented in Section 4. The results of simulation and experiment using the TMS320F28379D DSP kit for the methods of PM, PD and POD are presented in Section 5 with different magnitude values of the control signal. The effectiveness of the PM method is concluded in Section 6 when comparing the results of the three methods.

2. Five-level inverter model

The structure of a cascaded 5-level H-bridge three-phase inverter is shown in Figure 1. Where S_{xj} is the state ON/OFF of the switches as (1) with the phases x = a, b, c. The

switches S_{xj} are for the top switches and S'_{xj} are the bottom switches of the H-bridge, respectively.

$$S_{xj} + S'_{xj} = 1; \text{ with } j = 1 \div 4 \quad (1)$$

Table 1. Switching states of phase A

n	Sa1	Sa2	Sa3	Sa4	Output voltage
1	0	1	0	1	-2Vdc
2	0	1	0	0	-Vdc
3	0	0	0	0	0
4	1	0	0	0	+Vdc
5	1	0	1	0	+2Vdc

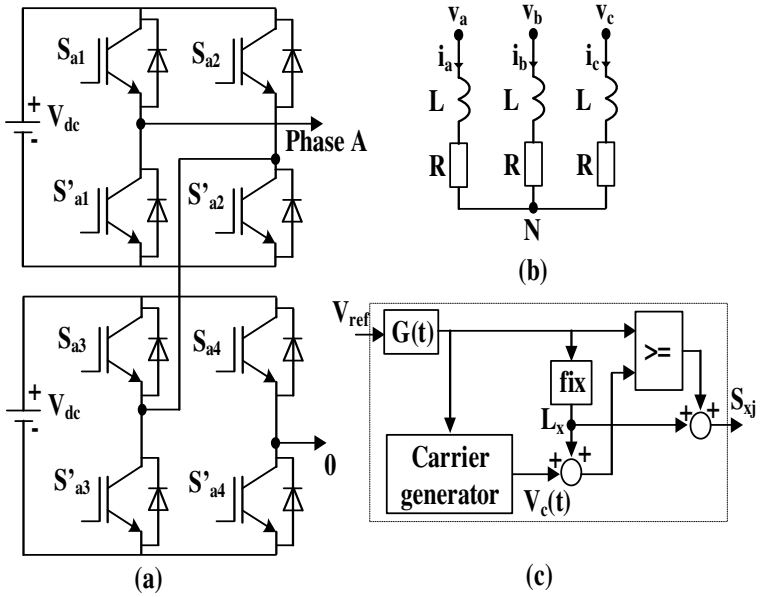

Figure 1. Structure of inverter (a) One-phase diagram of 5-level H-bridge 3-phase inverter (b) 3-phase load (c) Control principle of inverter.

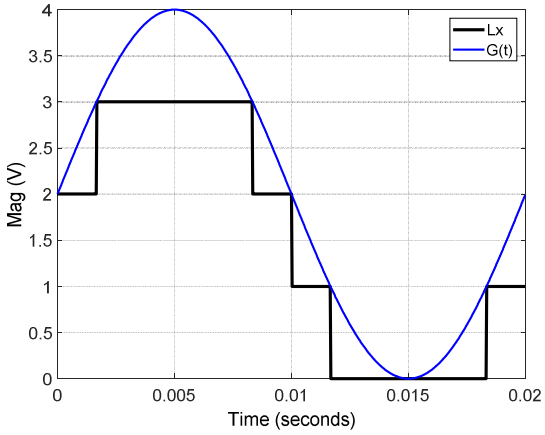

Figure 2. The quantization signal L_x.

The switching states of switches for phase A are described in Table I. Where the number of inverter levels is 5 and the dc voltage sources are the same, 5 levels of output voltage are $-2V_{dc}$, $-1V_{dc}$, 0, $+1V_{dc}$, and $+2V_{dc}$, respectively.

$$V_{ref}(t) = E_m \sin(\omega_m t);\ \omega_m = 2\pi f_m \quad (2)$$

$$G(t) = (V_{ref}(t) + 1) * \left(\frac{n-1}{2}\right) \quad (3)$$

$$L_x = \begin{cases} n-2 \text{ if } G(t) \geq n-2 \\ \text{fix}(G(t)), \text{ others} \end{cases} \quad (4)$$

When $V_{ref}(t)$ is the control signal with the magnitude from -1 to +1 and defined as (2). Where E_m (pu) is the magnitude of the control signal. Then, G(t) is the normalized control signal to make it appropriate for the number of levels as (3). L_x is the quantization level and showed in Figure 2. Where $0 \leq L_x \leq n-2$ is the integer part of G(t) and defined by (4).

3. Unmodulated carriers

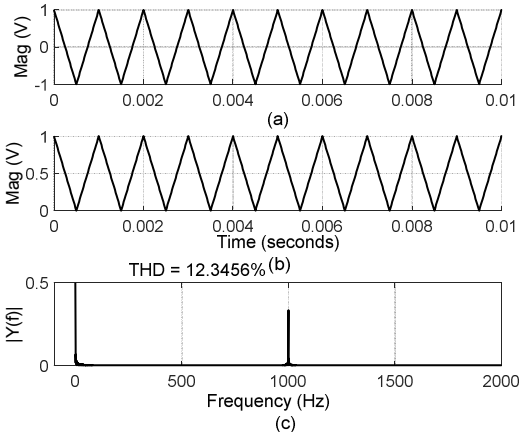

Figure 3. Unmodulated carriers with A_c=1 and f_c=1 kHz (a)

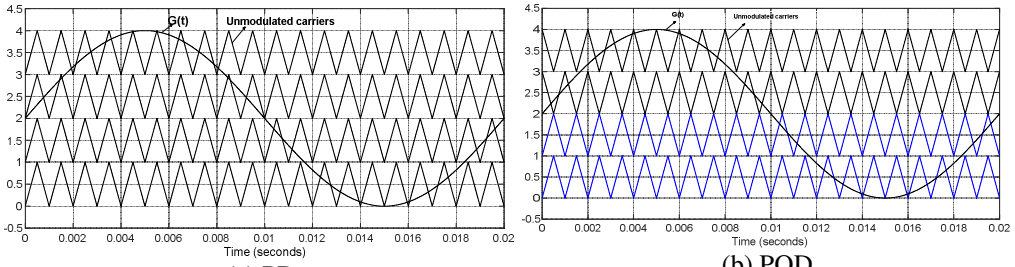

(a) PD (b) POD

Figure 4. Modulation methods with f_m=50 Hz, Ac=1 and fc=1 kHz

A high frequency carrier is described as follows.

$$e(t) = A_c \cos(\omega_c t + \varphi),\ \omega_c = 2\pi f_c \quad (5)$$

Then, the unmodulated carrier c(t) is as (6) and showed in Figure 3(a) with the phase φ=0, A_c=1, and the f_c=1 kHz. These carriers are also normalized in Figure 3(b). Then, the spectrum of these carriers in Figure 3(c) showed that the THD value is 12.34% in Figure 3(c). In addition, the individual harmonics concentrate on the frequency 1 kHz. This makes the magnitude of the individual harmonic significantly high.

$$c(t) = \frac{2}{\pi}\sin^{-1}\left(e(t)\right) = \frac{2}{\pi}\sin^{-1}\left(A_c\cos\left(\omega_c t + \varphi\right)\right) \quad (6)$$

$$V_c(t) = \frac{\max(c(t)) + c(t)}{\max(c(t)) + \min(c(t))} \quad (7)$$

The unmodulated carriers in Figure 3, (6), and (7) have also shown that they do not contain any information of the control signal V_{ref}. Therefore, it is very difficult to reproduce the control signal at the inverter output.

The methods using these unmodulated carriers such as PD and POD are also shown in Figures 4(a)-(b). Where the unmodulated carrier frequency is 1 kHz. Then, the common mode voltages of these methods are calculated as follows.

$$V_{CM} = \frac{v_a + v_b + v_c}{3} \quad (8)$$

The common mode voltages in Figure 5 have showed that the CMV magnitude of PD method in Figure 5(a) is equal to $+2V_{dc}/3$. This CMV magnitude value is twice as high as that of the POD method in Figure 5(b).

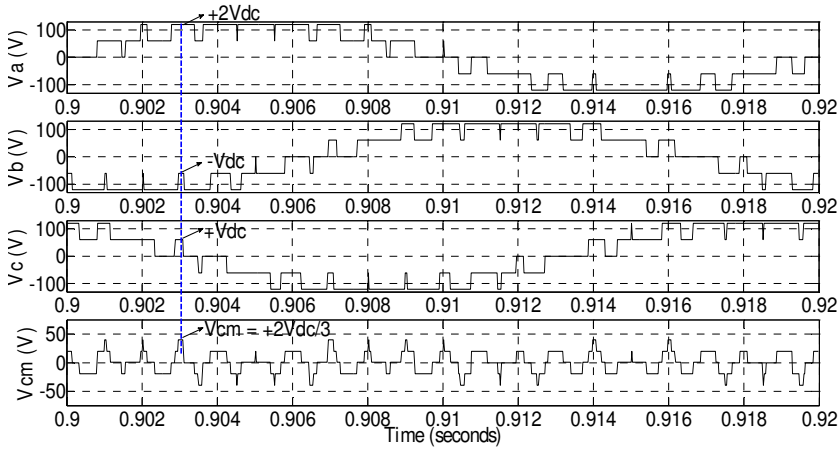

(a) PD

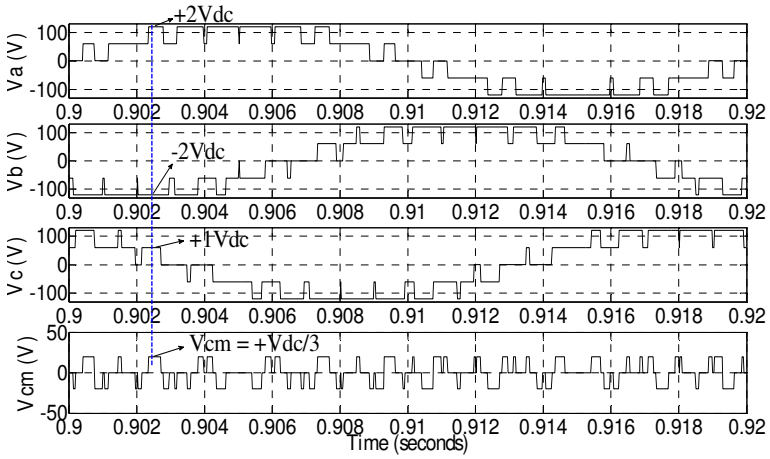

(b) POD

Figure 5. Common mode voltages (a) PD modulation (b) POD modulation

4. Proposed phase modulation of carriers

The phase modulation method of carriers is based on the control signal magnitude V_{ref}. From e(t) in (5), when the phase angle φ changes according to the magnitude of V_{ref}. We can obtain the phase modulation as follows.

$$e_{PM}(t) = A_c \cos\left[\omega_c t + \frac{m_{px}}{E_m} V_{ref}(t)\right] \quad (9)$$

$$\text{With angle } \theta = \omega_c t + \frac{m_{px}}{E_m} V_{ref}(t) \quad (10)$$

Then, the phase modulated carrier will be defined as follows.

$$c_{PM}(t) = \frac{2}{\pi}\sin^{-1}\left(A_c \cos\left[\omega_c t + \frac{m_{px}}{E_m} V_{ref}(t)\right]\right) \quad (11)$$

Where m_{px} is the phase modulation index according to the magnitude of Vref. The PM carriers are also normalized as follows.

$$V_{CPM}(t) = \frac{\max(c_{PM}(t)) + c_{PM}(t)}{\max(c_{PM}(t)) + \min(c_{PM}(t))} \quad (12)$$

The PM carriers in Figure 6 with m_{px}=10 have the THD as 11.4% in Figure 6(d) and lower than that of unmodulated carriers in Figure 3(c). Moreover, the spectrum spread in Figure 6(d) helps significantly reduce the magnitude of individual harmonics. This also helps reduce the acoustic noise of the inverters used for military and telecommunications.

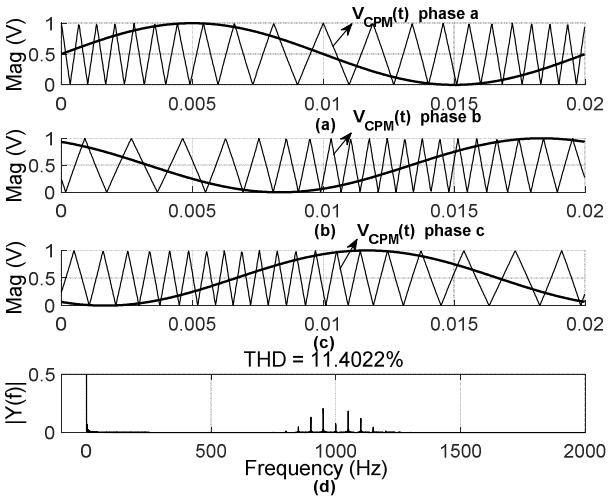

Figure 6. Phase modulated carriers with fc=1 kHz, m_{px}=10

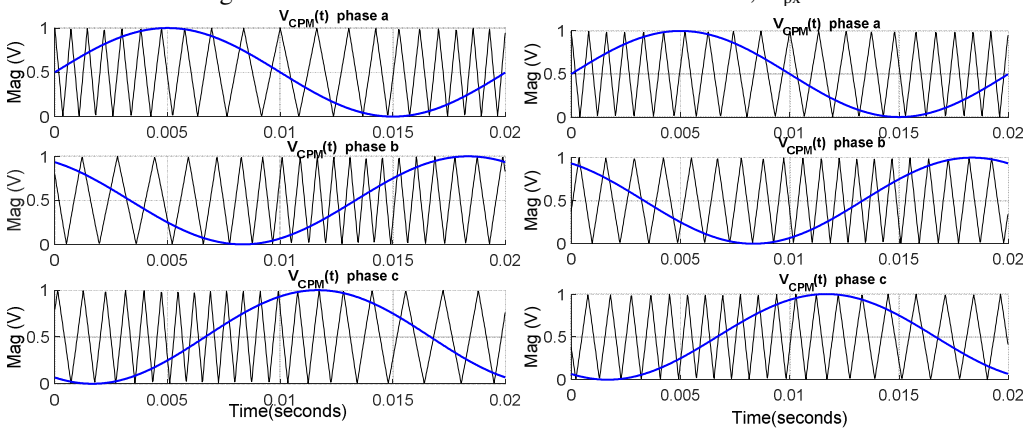

(a) m_{px}=8 (b) m_{px}=5.

Figure 7. Phase modulated carriers with fc=1 kHz

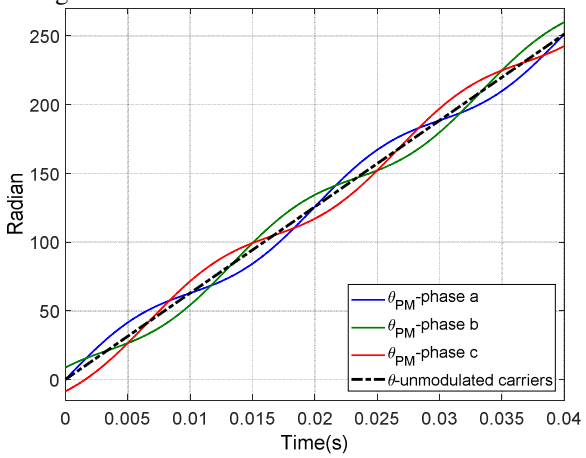

Figure 8. Angle θ of carriers with fm=50 Hz, fc=1 kHz, and m_{px}=10

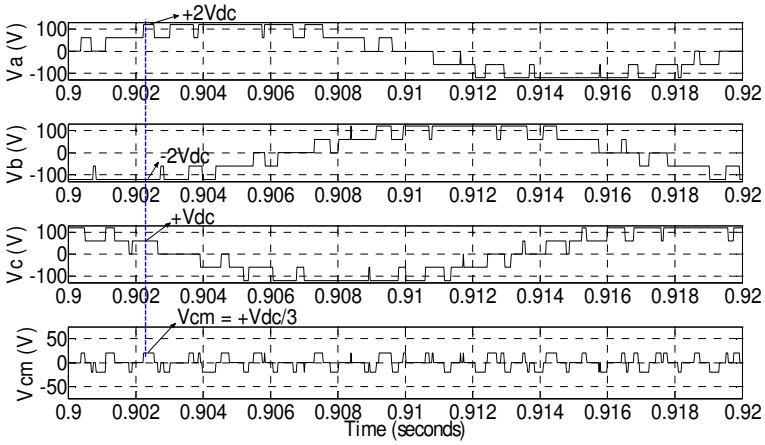

Figure 9. CMV of the PM method

The PM carriers with different values of m_{px} are showed in Figure 7. In addition, the change of the angle θ for PM carriers is also showed in Figure 8.

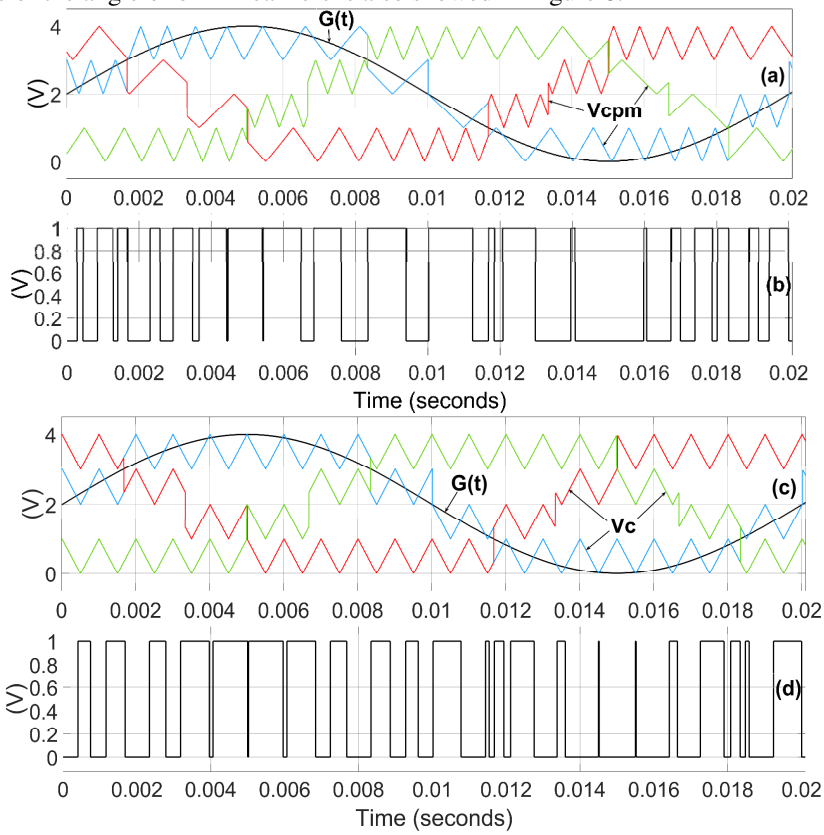

Figure 10. The switching pulses in one fundamental period with E_m=1, f_c=1 kHz, and f_m=50 Hz, (a)-(b) PM with m_{px}=10 (c)-(d) PD

The waveforms of the phase voltages in Figure 9 have showed that the CMV magnitude when using the PM carriers is equal to $V_{dc}/3$. This magnitude value is similar to that of the POD method in Figure 5(b).

In addition, the number of switching commutations of the PM method in Figures 10(a)-10(b) is 20 in each fundamental period of each phase, while that of the PD method in Figures 10(c)-10(d) is 22. Thus, the number of switching commutations of the PM method can reduce by 10% compared with that of the PD method. This can also help improve the efficiency of the inverters.

5. Results and discussion

The principle diagram of the simulation system is showed in Figure 11. Where the control signal $V_{ref}(t)$ consists of three phases with the magnitude E_m. The block Wrap, Wrap_to_zero in Simulink with the threshold of 0.02 s, is used to combine with the block Counter for counting the number of switching commutations in each fundamental period. The system parameters used for simulation and experiment are showed in Table 2.

Table 2. System parameters

Symbols	Parameters	Value
R	Load resistor	45 Ω
L	Load inductor	50 mH
Ts	Sample time	20 µs
T_D	Dead time	2 µs
f_c	Carrier frequency	2.5 kHz
m_{px}	Phase modulation index	2
V_{dc}	DC source voltage	60 V

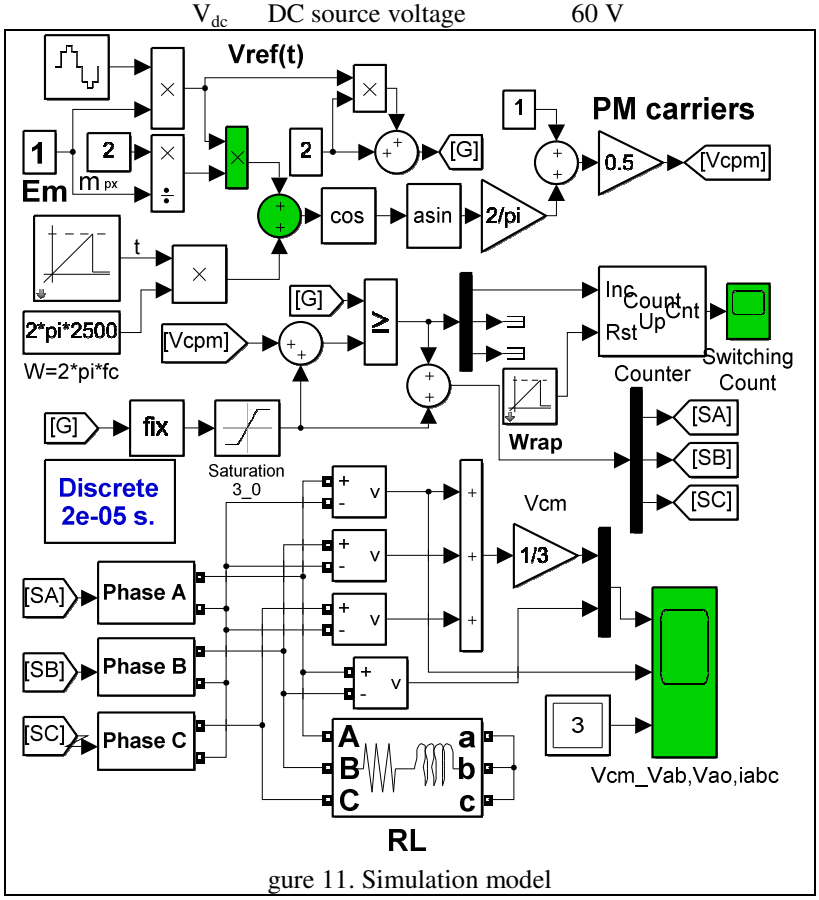

gure 11. Simulation model

5.1. Simulation

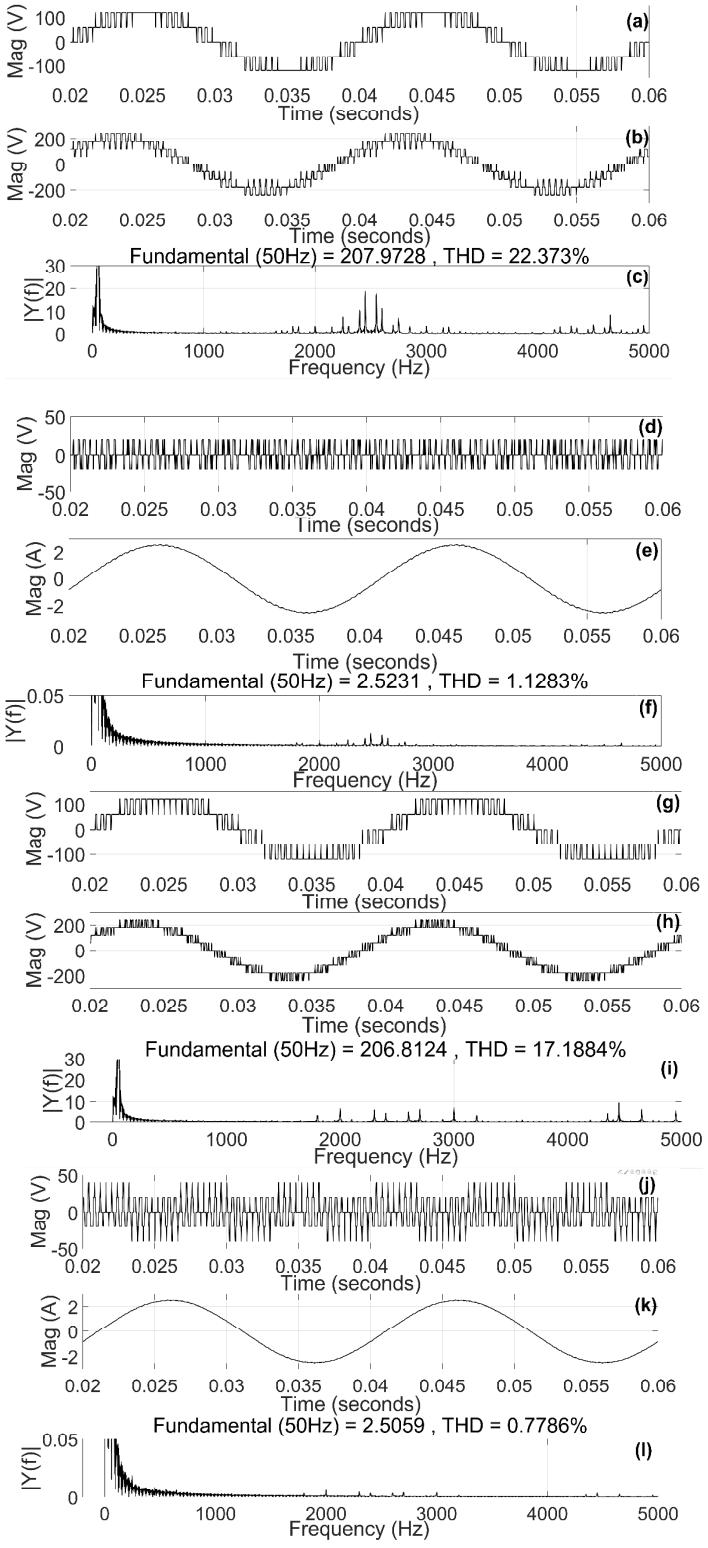

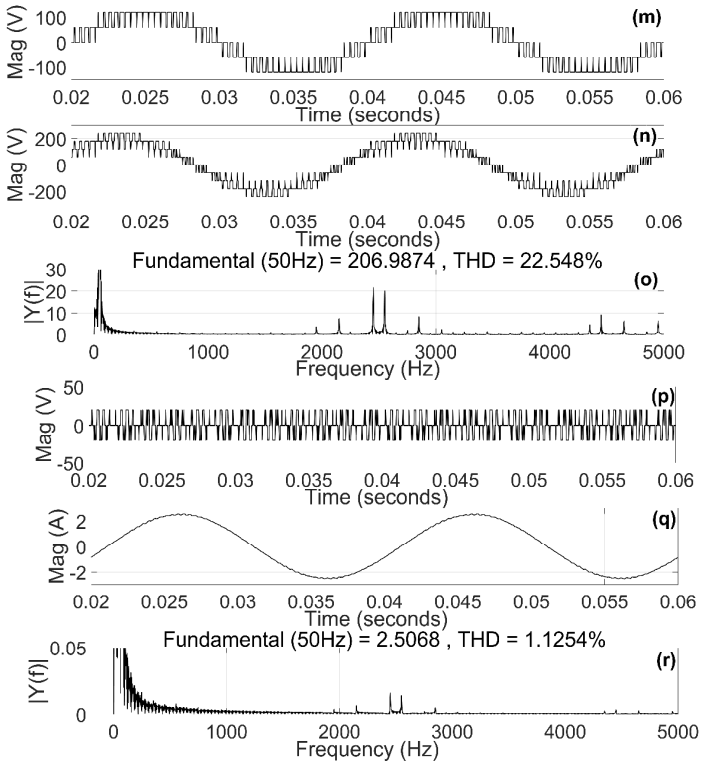

Figure 12. Phase voltage, line-line voltage V_{ab}, THD of V_{ab}, CMV, phase current, and THD of phase current when E_m=1 (a)-(f) PM (g)-(l) PD (m)-(r) POD.

The simulation results of three methods, PM, POD, and PD are showed in Figures 12-15 with different magnitude values of E_m, in per unit (pu). The quantities such as phase voltage, line-line voltage V_{ab}, spectrum and THD of V_{ab}, common mode voltage, phase current, and THD of phase current are shown in these figures from the top to the bottom respectively.

When the magnitude of E_m as 1 pu, the line-line voltage THD values of three methods in Figures 12(c), 12(i), and 12(o) are as 22.37%, 17.18%, and 22.54%, respectively. Thus, the line-line voltage THD value of the PD method is the smallest value and its CMV magnitude is the highest value and as $2V_{dc}/3$. While the CMV magnitude of the methods PM and POD is as $V_{dc}/3$. However, the voltage THD value of the PM method in Figure 12(c) is slightly lower than that of the POD method in Figure 12(o). In addition, the individual harmonic magnitude of the PM method near the frequency of 2.5 kHz is lower than 20% while that of the POD is higher than 20%. This has also helped increase the fundamental voltage magnitude of the PM method as 207.97 V, higher than that of the POD as 206.98 V. This also leads to the fundamental current magnitude of the PM method as 2.52 A in Figure 12(f), slightly higher than that of the POD method as 2.50 A in Figure 12(r).

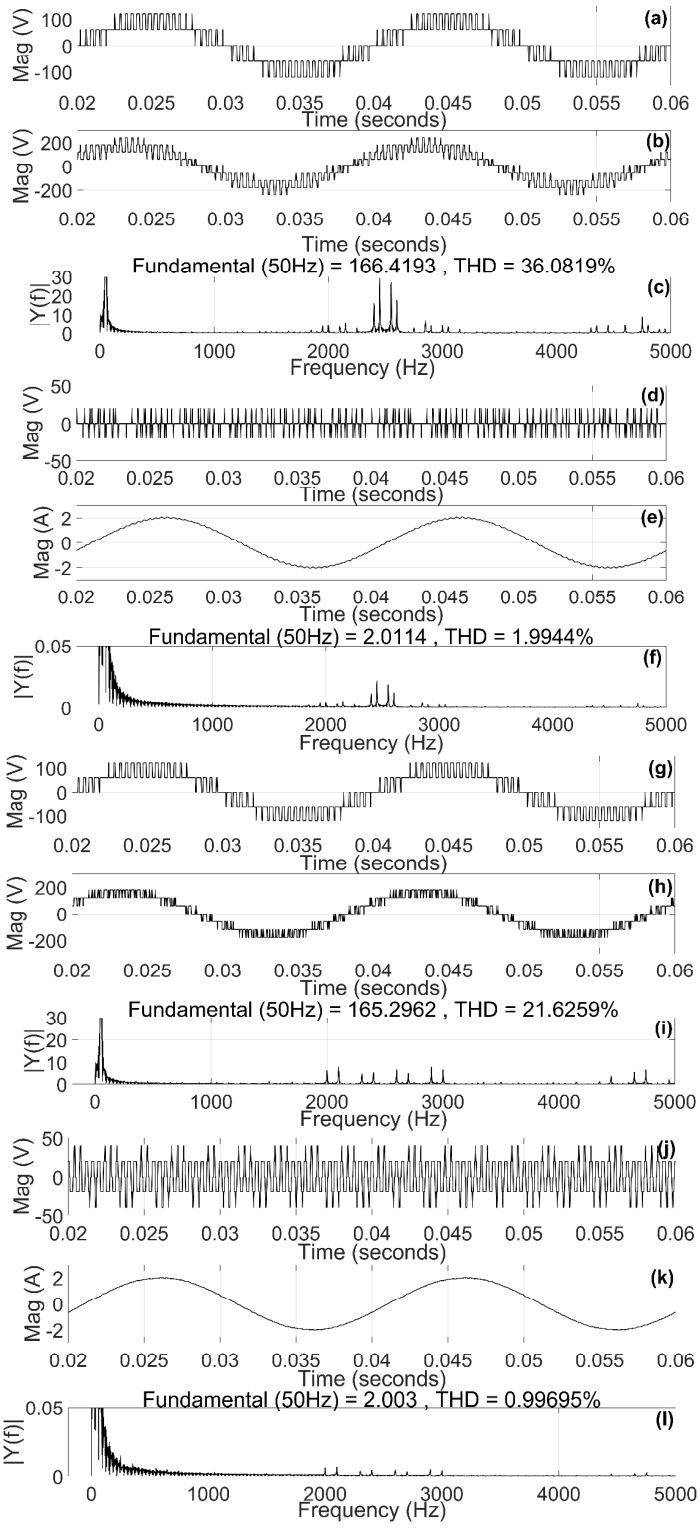
(a)
Meg (V)
Time (seconds)
(b)
Mag (V)
Time (seconds)
Fundamental (50Hz) = 166.4193 , THD = 36.0819%
(c)
|Y(f)|
Frequency (Hz)
(d)
Mag (V)
Time (seconds)
(e)
Mag (A)
Time (seconds)
Fundamental (50Hz) = 2.0114 , THD = 1.9944%
(f)
|Y(f)|
Frequency (Hz)
(g)
Mag (V)
Time (seconds)
(h)
Mag (V)
Time (seconds)
Fundamental (50Hz) = 165.2962 , THD = 21.6259%
(i)
|Y(f)|
Frequency (Hz)
(j)
Mag (V)
Time (seconds)
(k)
Mag (A)
Time (seconds)
Fundamental (50Hz) = 2.003 , THD = 0.99695%
(l)
|Y(f)|
Frequency (Hz)

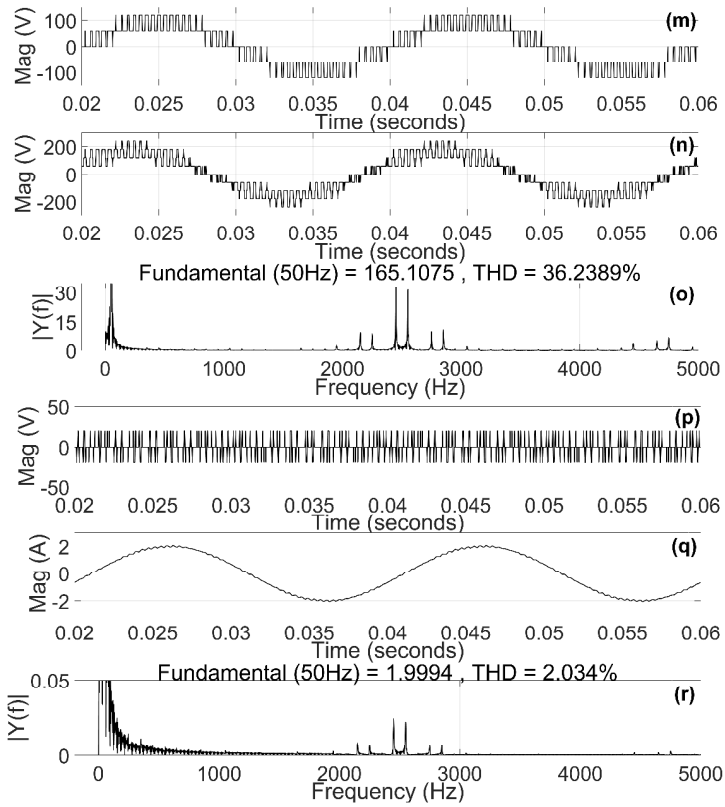

Figure 13. Phase voltage, line-line voltage Vab, THD of Vab, CMV, phase current, and THD of phase current when E_m=0.8 (a)-(f) PM (g)-(l) PD (m)-(r) POD.

Similarly, when the magnitude of E_m as 0.8, the line-line voltage THD values of three methods in Figures 13(c), 13(i), and 13(o) are as 36.0%, 21.6%, and 36.2%, respectively. The individual harmonic magnitude of the PM method near the frequency of 2.5 kHz in Figures 13(c) is lower than 30% while that of the POD is higher than 30% in Figures 13(o). The phase current waveforms of three methods are also shown in Figures 13(e), 13(k), and 13(q), respectively. Moreover, the fundamental current magnitude of the PM method in Figure 13 (f) is 2.01 A, higher than that of the POD method in Figure 13(r) as 1.99 A.

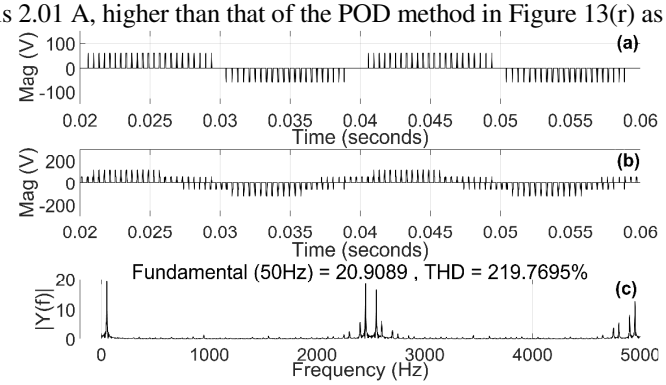

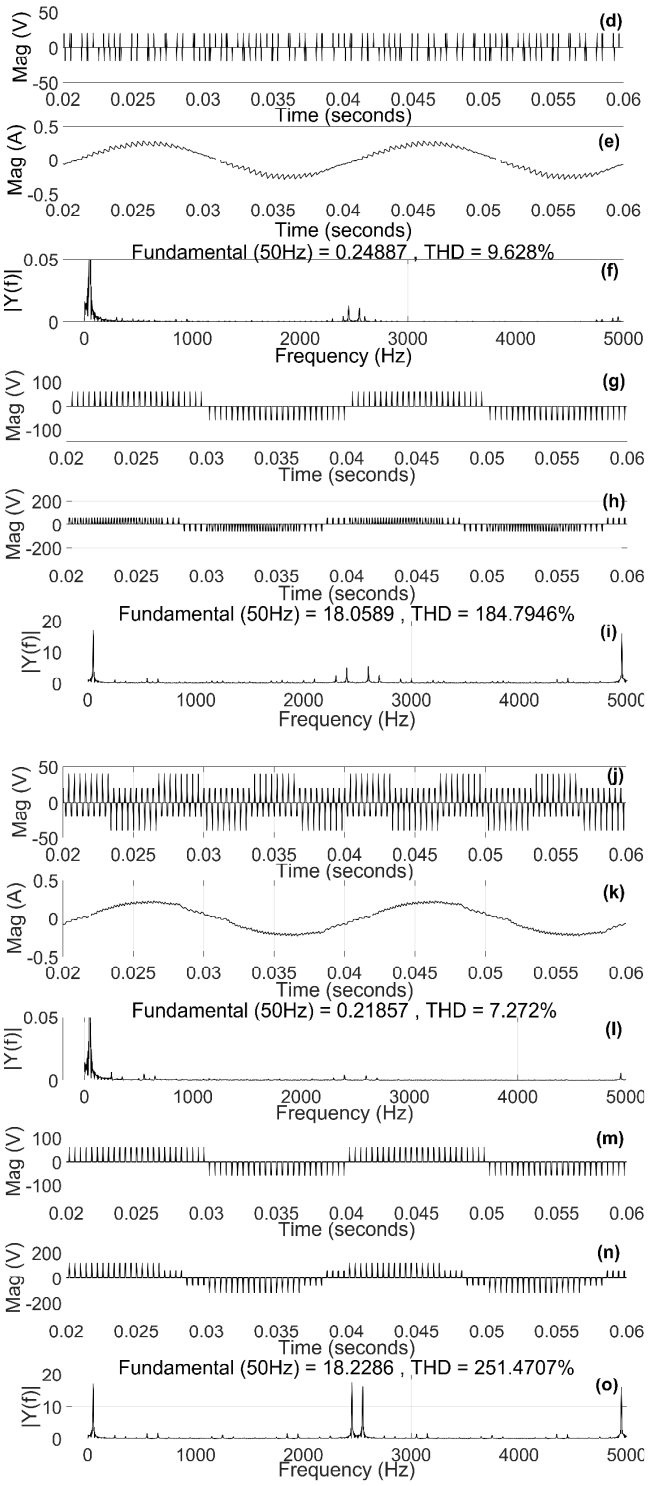
(d)
Mag (V)
Time (seconds)
(e)
Mag (A)
Time (seconds)
Fundamental (50Hz) = 0.24887 , THD = 9.628%
(f)
|Y(f)|
Frequency (Hz)
(g)
Mag (V)
Time (seconds)
(h)
Mag (V)
Time (seconds)
Fundamental (50Hz) = 18.0589 , THD = 184.7946%
(i)
|Y(f)|
Frequency (Hz)
(j)
Mag (V)
Time (seconds)
(k)
Mag (A)
Time (seconds)
Fundamental (50Hz) = 0.21857 , THD = 7.272%
(l)
|Y(f)|
Frequency (Hz)
(m)
Mag (V)
Time (seconds)
(n)
Mag (V)
Time (seconds)
Fundamental (50Hz) = 18.2286 , THD = 251.4707%
(o)
|Y(f)|
Frequency (Hz)

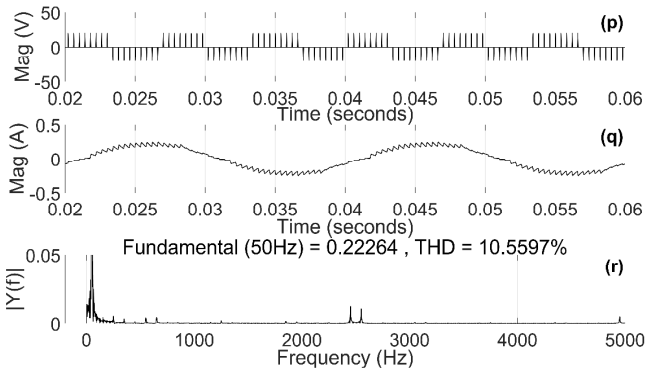

Figure 14. Phase voltage, line-line voltage Vab, THD of Vab, CMV, phase current, and THD of phase current when E_m=0.1 (a)-(f) PM (g)-(l) PD (m)-(r) POD.

When the magnitude of E_m as 0.1 pu, the line-line voltage THD values of three methods in Figures 14(c), 14(i), and 14(o) are as 219.76%, 184.79%, and 251.47% correspondingly. Thus, the line-line voltage THD value of the PD method is still the smallest and its CMV magnitude in Figure 14(j) is still the highest. The CMV magnitudes of the PM and POD methods in Figure 14(d) and Figure 14(p) are still as $V_{dc}/3$. Similar to the results mentioned in Figures 12-13, the voltage THD value of the PM method in Figure 14(c) is still lower than that of the POD method in Figure 14(o). This also leads to the fundamental current magnitude of the PM method as 0.248 A in Figure 14(f), slightly higher than that of the POD method as 0.222 A in Figure 14(r).

The THD values of the line-line voltage V_{ab} and the phase current according to different values of the magnitude E_m are showed in Figures 15(a)-15(b). Moreover, the weighted THD value versus the magnitude E_m is also surveyed in Figure 15(c). This has validated the robustness of the PM method for different load types of inverters.

Therefore, the CMV magnitude of the PM method is equal to that of the POD. However, the voltage THD value of the PM method is always lower than that of the POD method.

In addition, the number of switching commutations in each fundamental period of one phase is also showed in Figure 15(d). This result has also showed that the number of switching commutations of the PM method significantly reduces compared with those of the PD and POD methods. This helps the PM method reduce switching loss and improve the efficiency of the inverters.

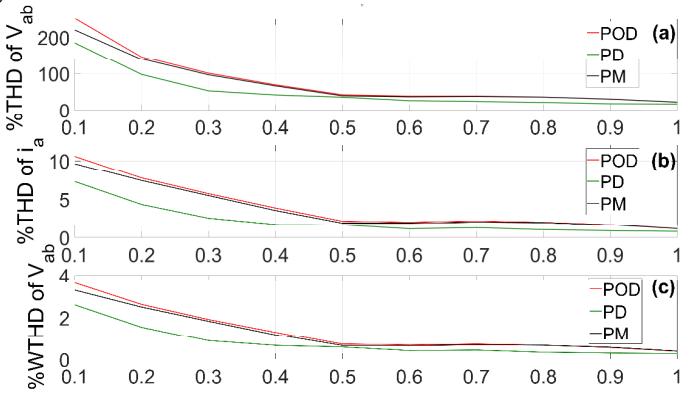

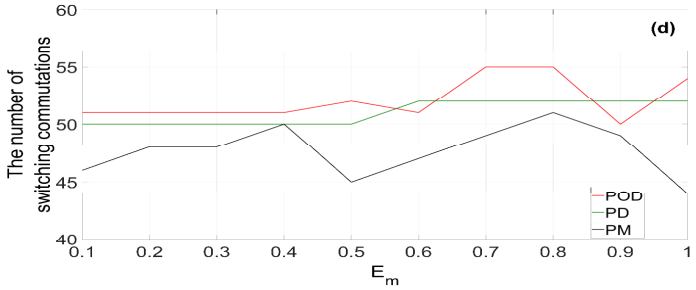

Figure 15. THD values and the number of switching commutations for one-phase versus E_m (pu).

5.2. Experiment

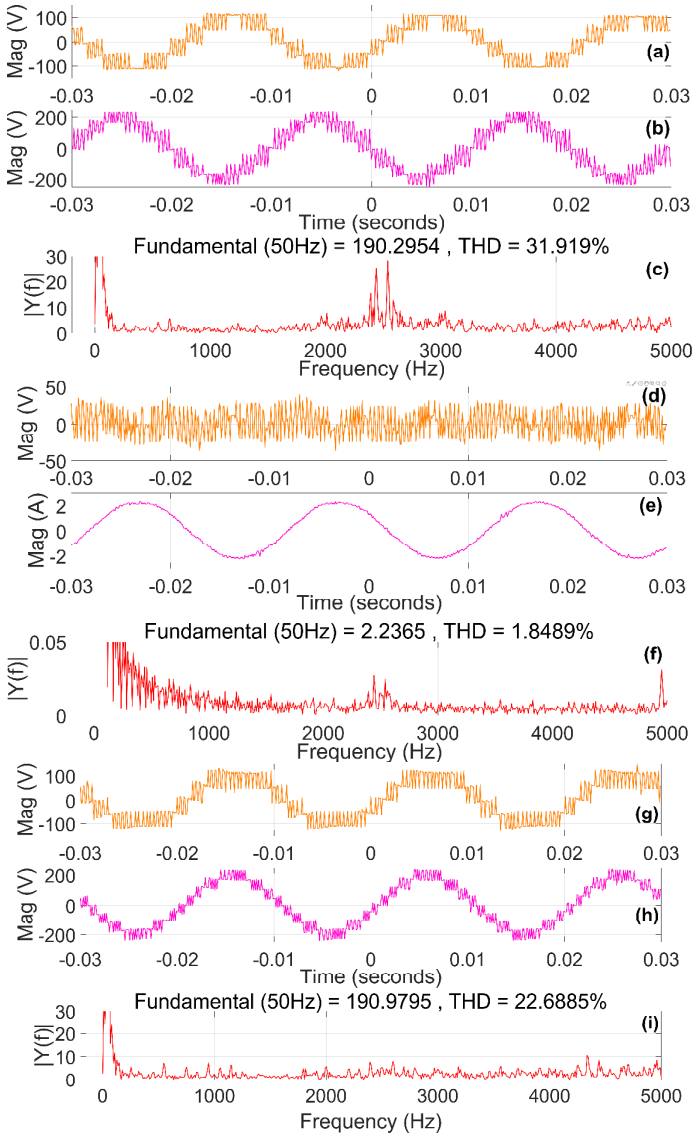

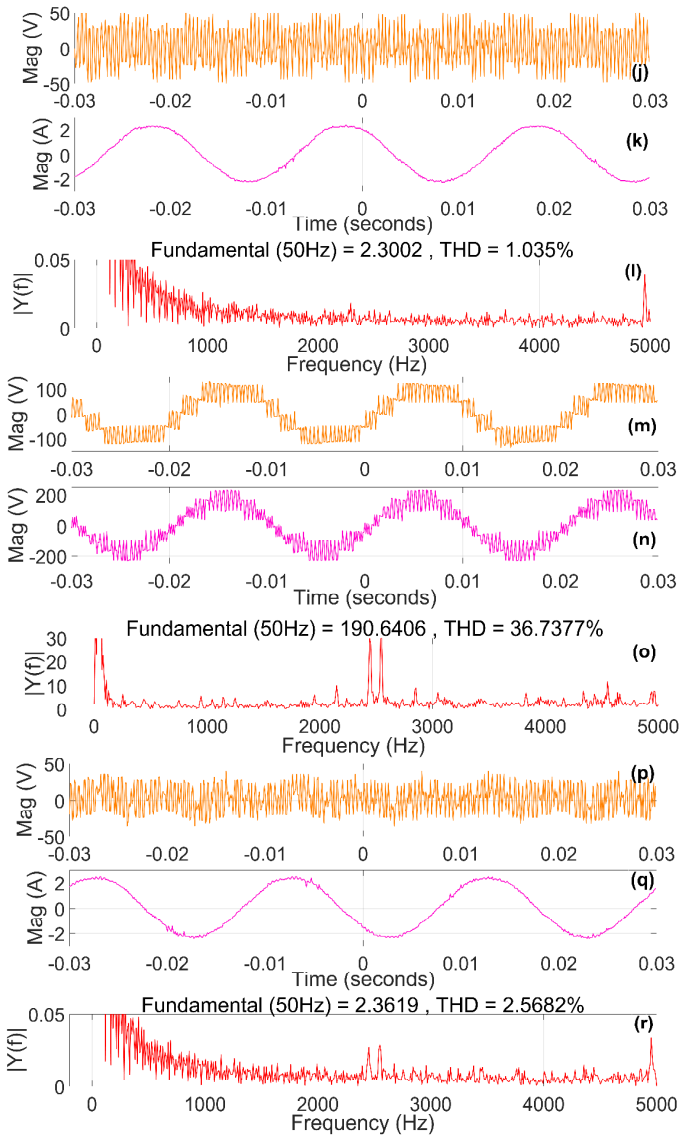

Figure 16. Phase voltage, line-line voltage Vab, THD of Vab, CMV, phase current, and THD of phase current when Em=1 (a)-(f) PM (g)-(l) PD (m)-(r) POD.

The experiment results in this paper are based on a 32-bit fixed-point TMS320F28379D DSP platform. The measurements and waveforms were taken with the Tektronix MSO-2024B oscilloscope in the waveform data. Then, these data are used for plotting and FFT analysis by using tools of MATLAB and showed in Figures 16-18.

Similar to the simulation, the experiment results are also surveyed with different values of control signal magnitude.

Figures 16(a)-16(f) have showed the experiment result of the PM method when E_m as 1 has the voltage THD as 31.9%, while those of the PD and POD are 22.6% and 36.7% in Figures 16(g)-16(l) and Figures 16(m)-16(r), respectively. Thus, the voltage THD value of the PM method is lower than that of the POD method. In addition, the individual harmonic magnitude near the frequency of 2.5 kHz in Figure 16(c) of the PM method is lower than 30% while that of the POD in Figure 16(o) is higher than 30%.

Because the dc voltage sources in the reality of the experiment are not the same value as 60 V, the fundamental voltage magnitude values in Figures 16(c), 16(i), and 16(o) are about 190 V. These values are slightly lower than those of the simulation results in Figures 12(c), 12(i), and 12(o) about 207 V, respectively. This makes the fundamental current magnitude values in Figures 16(f), 16(l), and 16(r) about 2.3 A and lower than those of the simulation in Figures 12(f), 12(l), and 12(r) about 2.5 A, respectively. However, the phase current THD of the PM method in Figure 16(f) is as 1.84%, still lower than that of the POD method in Figure 16(r) as 2.56%, although the CMV magnitudes of these methods in Figures 16(d) and 16(p) are the same as $V_{dc}/3$.

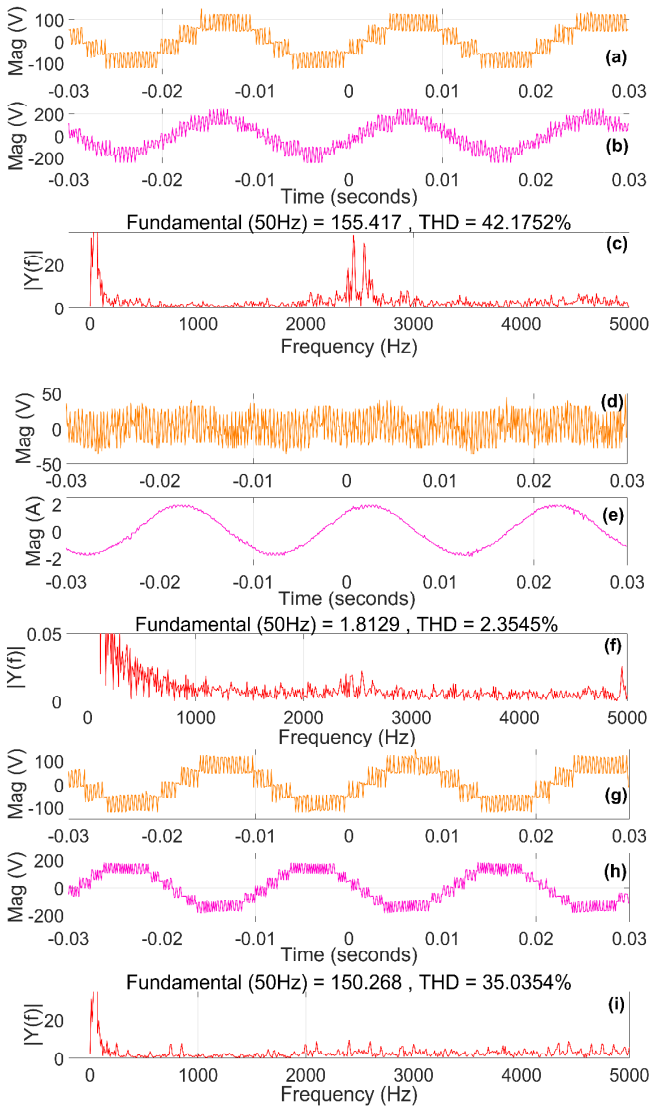

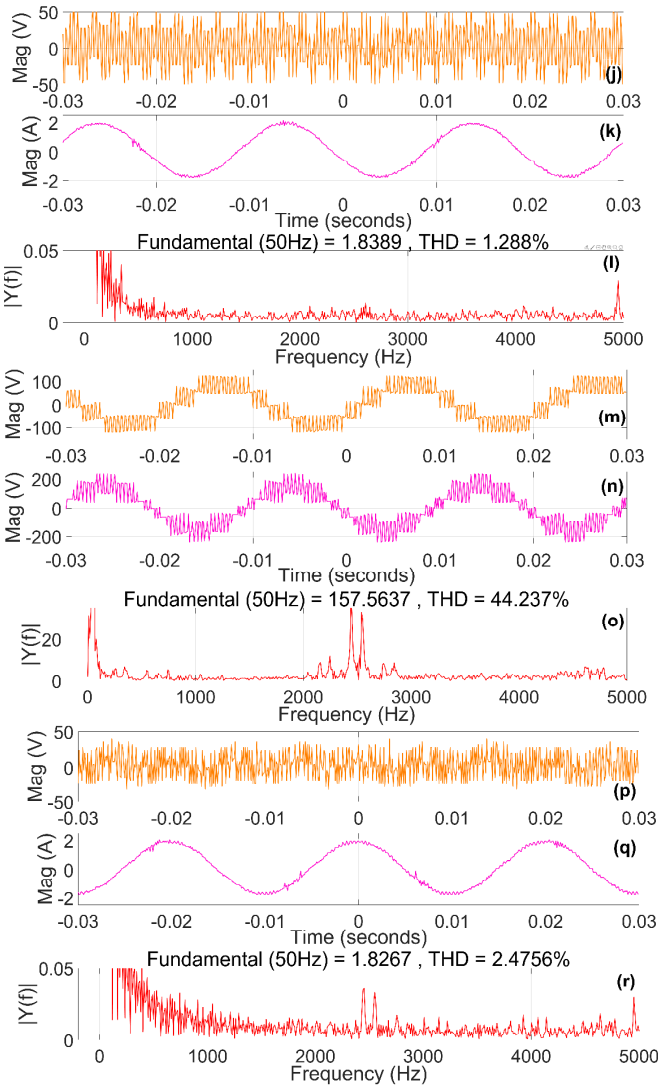

Figure 17. Phase voltage, line-line voltage Vab, THD of Vab, CMV, phase current, and THD of phase current when E_m=0.8 (a)-(f) PM (g)-(l) PD (m)-(r) POD.

When E_m as 0.8 pu, the experiment results of the PM method are showed in Figures 17(a)-17(f). Those of the PD and POD methods are showed in Figures 17(g)-17(l) and Figures 17(m)-17(r), respectively. The voltage THD values of the three methods are 42.1%, 35.0%, and 44.2%, correspondingly. Similarly, the phase current THD values of these methods are 2.35%, 1.28%, and 2.47%, respectively. The CMV magnitudes of the PM and POD methods in Figures 17(d) and 17(p) are still the same as $V_{dc}/3$ while that of the PD in Figure 17(j) is still as $2*V_{dc}/3$.

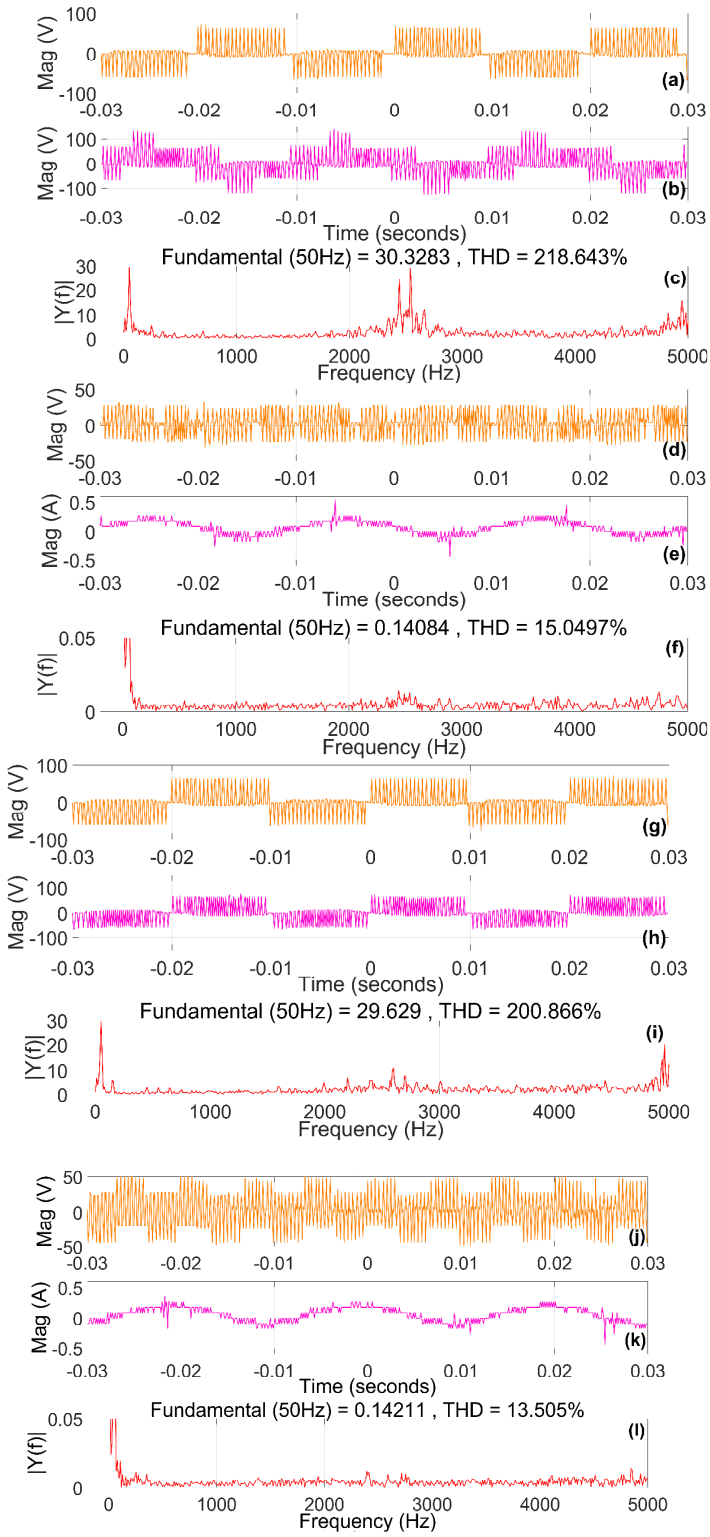
Mag (V)
(a)
(b)
Time (seconds)
Fundamental (50Hz) = 30.3283 , THD = 218.643%
|Y(f)|
(c)
Frequency (Hz)
Mag (A)
(d)
(e)
Fundamental (50Hz) = 0.14084 , THD = 15.0497%
(f)
(g)
(h)
Fundamental (50Hz) = 29.629 , THD = 200.866%
(i)
(j)
(k)
Fundamental (50Hz) = 0.14211 , THD = 13.505%
(l)

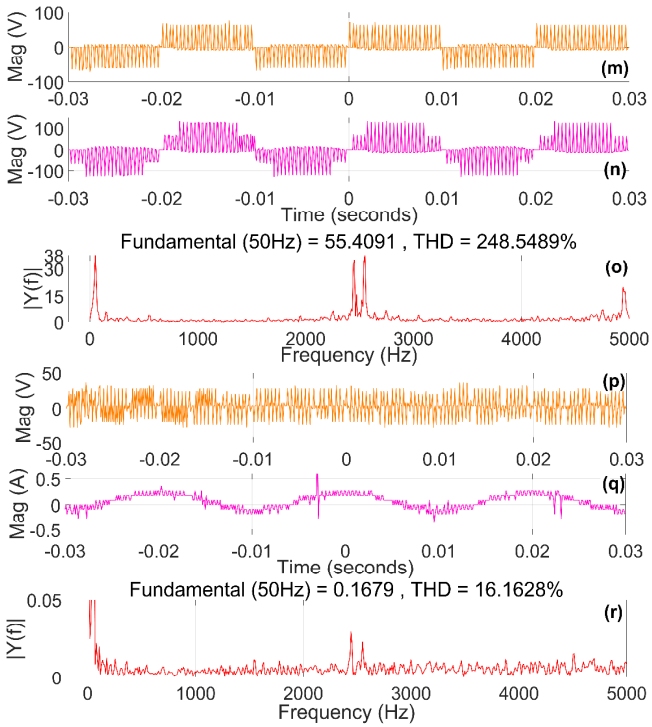

Figure 18. Phase voltage, line-line voltage Vab, THD of Vab, CMV, phase current, and THD of phase current when E_m=0.1 (a)-(f) PM (g)-(l) PD (m)-(r) POD.

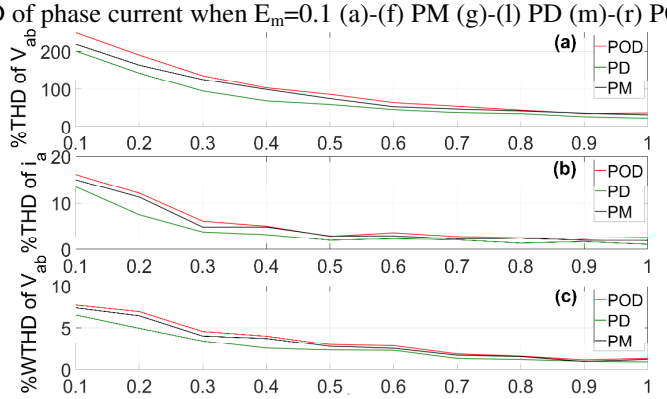

Figure 19. THD values versus the different magnitudes of E_m

The experiment results in Figure 18 of three methods have also showed that the voltage THD value of the PM method is lower than that of the POD method. The current THD value of the POD is also higher than that of the PM method.

In addition, the THD values of the line-line voltage V_{ab} and the phase current according to different values of the magnitude E_m are also showed in Figures 19(a)-(b). Moreover, the weighted THD value versus the magnitude E_m is also surveyed in Figure 19(c). Therefore, the CMV magnitude of the PM method is equal to that of the POD. However, the voltage and current THD values of the PM method are always lower than those of the POD method while these methods offer the same CMV magnitude.

6. Conclusion

This paper has proposed a carrier phase modulation method for the cascaded multilevel three-phase inverters. The phase of carrier in the proposed method is simply modulated according to the control signal magnitude. The PM carriers contain the information of the control signal. Thus, these carriers help easily reproduce the entire control signal at the output of inverters. This method also helps increase the inverter output fundamental voltage magnitude. Then, the inverter efficiency is also increased. The voltage and current THD values and the CMV magnitudes have been evaluated quantitatively. The proposed method does not require more any hardware.

In addition, the number of switching commutations of the PM method is lower than those of the PD and POD methods. This helps decrease the switching loss and improve the efficiency of inverters.

The simulation and experiment results based on the system of a cascaded 5-level three-phase inverter have also validated the effectiveness of the proposed PM method compared with that of the PD and POD methods using unmodulated carriers.

Acknowledgment

This work belongs to the project 2022 funded by Ho Chi Minh City University of Technology and Education, Vietnam.

References

[1] J. Rodriguez, L. Jih-Sheng, and Z. P. Fang, "Multilevel Inverters: A Survey of Topologies, Controls, and Applications," *IEEE Trans. Ind. Electron.*, vol. 49, no. 4, pp. 724–738, 2002, doi: 10.1142/S1793557108000072.

[2] M. M. Hasan, A. Abu-Siada, S. M. Islam, and M. S. A. Dahidah, "A New Cascaded Multilevel Inverter Topology with Galvanic Isolation," *IEEE Trans. Ind. Appl.*, vol. 54, no. 4, pp. 3463–3472, 2018, doi: 10.1109/TIA.2018.2818061.

[3] M. D. Siddique, S. Mekhilef, N. M. Shah, and M. A. Memon, "Optimal Design of a New Cascaded Multilevel Inverter Topology With Reduced Switch Count," *IEEE Access*, vol. 7, pp. 24498–24510, 2019, doi: 10.1109/ACCESS.2019.2890872.

[4] J. Zeng *et al.*, "Dynamic space vector based discontinuous PWM for three-level inverters," *Int. J. Electr. Power Energy Syst.*, vol. 117, no. October 2019, p. 105638, 2020, doi: 10.1016/j.ijepes.2019.105638.

[5] G. Schettino, F. Viola, A. O. Di Tommaso, P. Livreri, and R. Miceli, "Experimental Validation of a Novel Method for Harmonic Mitigation for a Three-Phase Five-Level Cascaded H-Bridges Inverter," *IEEE Trans. Ind. Appl.*, vol. 55, no. 6, pp. 6089–6101, 2019, doi: 10.1109/TIA.2019.2933522.

[6] A. K. Yadav, K. Gopakumar, R. Krishna Raj, L. Umanand, S. Bhattacharya, and W. Jarzyna, "A Hybrid 7-Level Inverter Using Low-Voltage Devices and Operation with Single DC-Link," *IEEE Trans. Power Electron.*, vol. 34, no. 10, pp. 9844–9853, 2019, doi: 10.1109/TPEL.2018.2890371.

[7] N. Raj, T. Kale, A. Anand, G. Jagadanand, and S. George, "Switch fault detection and diagnosis in space vector modulated cascaded H-bridge multilevel inverter," *Int. J. Electron.*, vol. 105, no. 12, pp. 1977–1992, 2018, doi: 10.1080/00207217.2018.1494327.

[8] P. Chaturvedi, *Conventional multilevel inverter: Topologies and control strategies*. Elsevier Inc., 2018.

[9] A. K. Panda and Y. Suresh, "Research on cascade multilevel inverter with single DC source by using three-phase transformers," *Int. J. Electr. Power Energy Syst.*, vol. 40, no. 1, pp. 9–20, 2012, doi: 10.1016/j.ijepes.2011.12.012.

[10] A. Iqbal, M. Meraj, M. Tariq, K. A. Lodi, A. I. Maswood, and S. Rahman, "Experimental Investigation and Comparative Evaluation of Standard Level Shifted Multi-Carrier Modulation Schemes with a Constraint GA Based SHE Techniques for a Seven-Level PUC Inverter," *IEEE Access*, vol. 7, pp. 100605–100617, 2019, doi: 10.1109/ACCESS.2019.2928693.

[11] A. Hassan, X. Yang, and W. Chen, "A Multi-Cell 21-Level Hybrid Multilevel Inverter Synthesizes a Reduced Number of Components with Voltage Boosting Property," *IEEE Access*, vol. 8, pp. 224439–224451, 2020, doi: 10.1109/ACCESS.2020.3044268.

[12] C. Wang, Y. He, Y. Wang, and J. Liu, "Research of the equivalent relationship between the space vector and the triangular carrier-based PWM modulation strategies in the flying capacitor multilevel inverters," *Int. J. Electron.*, vol. 106, no. 3, pp. 395–414, 2019, doi: 10.1080/00207217.2018.1540061.

[13] H. J. Kim, H. D. Lee, and S. K. Sul, "A new PWM strategy for common-mode voltage reduction in neutral-point-clamped inverter-fed ac motor drives," *IEEE Trans. Ind. Appl.*, vol. 37, no. 6, pp. 1840–1845, 2001, doi: 10.1109/28.968199.

[14] A. K. Gupta and A. M. Khambadkone, "A space vector modulation scheme to reduce common mode voltage for cascaded multilevel inverters," *IEEE Trans. Power Electron.*, vol. 22, no. 5, pp. 1672–1681, 2007, doi: 10.1109/TPEL.2007.904195.

[15] H. Zhang, A. Von Jouanne, S. Dai, A. K. Wallace, and F. Wang, "Multilevel inverter modulation schemes to eliminate common-mode voltages," *IEEE Trans. Ind. Appl.*, vol. 36, no. 6, pp. 1645–1653, 2000, doi: 10.1109/28.887217.

[16] P. C. Loh, D. G. Holmes, Y. Fukuta, and T. A. Lipo, "Reduced common-mode modulation strategies for cascaded multilevel inverters," *IEEE Trans. Ind. Appl.*, vol. 39, no. 5, pp. 1386–1395, 2003, doi: 10.1109/TIA.2003.816547.

[17] A. Alexander Stonier, "Design and development of high performance solar photovoltaic inverter with advanced modulation techniques to improve power quality," *Int. J. Electron.*, vol. 104, no. 2, pp. 174–189, 2017, doi: 10.1080/00207217.2016.1196746.

[18] Yaskawa Electric America Inc., "Application Note Motor Bearing Current Phenomenon Rev : 08-08." pp. 1–9, 2008, [Online]. Available: https://www.yaskawa.com/downloads/search-index/details?showType=details&docnum=AN.AFD.17.

[19] and G. S. Doyle Busse, Jay Erdman, Russel J. Kerkman, Dave Schlegel, "Bearing Currents and Their Relationship to PWM Drives," *IEEE Trans. Power Electron.*, vol. 12, no. 2, pp. 243–252, 1997, doi: 10.1109/63.558735.

[20] C. C. Hou, C. C. Shih, P. T. Cheng, and A. M. Hava, "Common-mode voltage reduction pulsewidth modulation techniques for three-phase grid-connected converters," *IEEE Trans. Power Electron.*, vol. 28, no. 4, pp. 1971–1979, 2013, doi: 10.1109/TPEL.2012.2196712.

[21] J. Rodríguez, J. Pontt, P. Correa, P. Cortés, and C. Silva, "A new modulation method to reduce common-mode voltages in multilevel inverters," *IEEE Trans. Ind. Electron.*, vol. 51, no. 4, pp. 834–839, 2004, doi: 10.1109/TIE.2004.831735.

[22] P. C. Loh, D. G. Holmes, Y. Fukuta, and T. A. Lipo, "A reduced common mode hysteresis current regulation strategy for multilevel inverters," *IEEE Trans. Power Electron.*, vol. 19, no. 1, pp. 192–200, 2004, doi: 10.1109/TPEL.2003.820539.

[23] A. M. Hava and E. Ün, "Performance analysis of reduced common-mode voltage PWM methods and comparison with standard PWM methods for three-phase voltage-source inverters," *IEEE Trans. Power Electron.*, vol. 24, no. 1, pp. 241–252, 2009, doi: 10.1109/TPEL.2008.2005719.

[24] V. Naumanen, J. Korhonen, J. Luukko, and P. Silventoinen, "Multilevel inverter modulation method to reduce common-mode voltage and overvoltage at the motor terminals," in *2010 IEEE 26th Convention of Electrical and Electronics Engineers in Israel, IEEEI 2010*, 2010, pp. 296–300, doi: 10.1109/EEEI.2010.5662221.

[25] M. C. Di Piazza, M. Luna, and G. Vitale, "EMI Reduction in DC-Fed Electric Drives by Active Common-Mode Compensator," *IEEE Trans. Electromagn. Compat.*, vol. 56, no. 5, pp. 1067–1076, 2014, doi: 10.1109/TEMC.2014.2304836.

[26] Z. Zhao, Y. Zhong, H. Gao, L. Yuan, and T. Lu, "Hybrid selective harmonic elimination PWM for common-mode voltage reduction in three-level neutral-point-clamped inverters for variable speed induction drives," *IEEE Trans. Power Electron.*, vol. 27, no. 3, pp. 1152–1158, 2012, doi: 10.1109/TPEL.2011.2162591.

[27] K. Tian, J. Wang, B. Wu, D. Xu, Z. Cheng, and N. R. Zargari, "A virtual space vector modulation technique for the reduction of common-mode voltages in both magnitude and third-order component," *IEEE Trans. Power Electron.*, vol. 31, no. 1, pp. 839–848, 2016, doi: 10.1109/TPEL.2015.2408812.

[28] N. Boudjerda, A. Boudouda, M. Melit, B. Nekhoul, K. El Khamlichi Drissi, and K. Kerroum, "Spread spectrum in three-phase inverter by an optimised dual randomised PWM technique," *Int. J. Electron.*, vol. 101, no. 3, pp. 308–324, 2014, doi: 10.1080/00207217.2013.780299.

[29] J. Huang, Q. Liu, X. Wang, and K. Li, "A Carrier-Based Modulation Scheme to Reduce the Third Harmonic Component of Common-Mode Voltage in a Three-Phase Inverter under High DC Voltage Utilization," *IEEE Trans. Ind. Electron.*, vol. 65, no. 3, pp. 1931–1940, 2018, doi: 10.1109/TIE.2017.2745439.

[30] A. Ruiz-Gonzalez, M. Meco-Gutierrez, J. R. Heredia-Larrubia, F. Perez-Hidalgo, and F. Vargas-Merino, "Pulse width modulation technique with harmonic injection in the modulating wave and discontinuous frequency modulation for the carrier wave to reduce vibrations in asynchronous machines," *IET Power Electron.*, vol. 12, no. 11, pp. 2865–2872, 2019, doi: 10.1049/iet-pel.2018.5178.

[31] P. Palanivel and S. S. Dash, "Analysis of THD and output voltage performance for cascaded multilevel inverter using carrier pulse width modulation techniques," *IET Power Electron.*, vol. 4, no. 8, pp. 951–958, 2011, doi: 10.1049/iet-pel.2010.0332.

[32] R. Xue, H. Yu, and Q. Cheng, "Adaptive Coded Modulation Based on Continuous Phase Modulation for Inter-Satellite Links of Global Navigation Satellite Systems," *IEEE Access*, vol. 6, no. c, pp. 20652–20662, 2018, doi: 10.1109/ACCESS.2018.2825255.

[33] C. He, B. Lin, Q. Chen, A. Cao, J. Chen, and R. Jin, "Periodic Phase Modulation Method for Fast Diagnosis of Phased Array," *IEEE Trans. Antennas Propag.*, vol. 69, no. 2, pp. 1184–1187, 2021, doi: 10.1109/TAP.2020.3021750.
[34] T. J. Rouphael, "Common Digital Modulation Methods," in *Signal Processing for Software-Defined Radio*, 2009, pp. 25–85.
[35] J. Mon *et al.*, "EMI reduction by means of switching frequency modulation with variable delay in power supplies," *Int. J. Electron.*, vol. 99, no. 1, pp. 103–112, 2012, doi: 10.1080/00207217.2011.610026.
[36] T. J. Rouphael, "Chapter 2. Common Analog Modulation and Pulse-Shaping Methods," in *RF and Digital Signal Processing for Software-Defined Radio*, H. Helms, R. Roumeliotis, H. Scherer, R. S. Kumar, and A. McGee, Eds. Elsevier Inc, 2009, pp. 7–24.
[37] H. Wang *et al.*, "Suppression of backscattering-induced noise in a resonator optic gyro by the dual-frequency modulation method," *Opt. Commun.*, vol. 459, no. September 2019, pp. 1–5, 2020, doi: 10.1016/j.optcom.2019.124766.
[38] M. Plonus, "Digital systems," in *Electronics and Communications for Scientists and Engineers*, 2nd ed., Elsevier, 2020, pp. 402–413.
[39] M. Jamil, "Carrier-based modulation strategies for a neutral point clamped inverter," *Int. J. Electron.*, vol. 95, no. 12, pp. 1293–1303, 2008, doi: 10.1080/00207210802524294.
[40] S. Chitra and K. R. Valluvan, "Design and implementation of cascaded H-Bridge multilevel inverter using FPGA with multiple carrier phase disposition modulation scheme," *Microprocess. Microsyst.*, vol. 76, pp. 1–8, 2020, doi: 10.1016/j.micpro.2020.103108.